Crack Propagation in Concrete Using Meshless Method

N. Sageresan and R. Drathi

Abstract: Crack propagation in concrete is computed with a simplified meshless method. The material is elastic of Neo-Hookian type until fracture. Then a discrete cohesive crack method is used. In the cohesive crack method, cohesive segments are introduced at the meshless nodes. No representation of the crack surface is needed. The method is well-suited for concrete since concrete develops many cracks. Mesh independent results are obtained due to the cohesive model that takes into account the correct energy dissipation during crack opening. We show the accuracy of our method by comparison to experimental data.

Keyword: concrete, crack, fracture

1 Introduction

Initiated in 1961 by Kaplan (1961), the study of fracture mechanics has progressed by the turn of the century quite far. Kesler, Naus, and Lott (1972) showed that the classical linear elastic fracture mechanics (LEFM) of sharp cracks was inadequate for normal concrete structures. This conclusion was supported in 1972 by the results of Walsh (1972, 1976) who tested geometrically similar notched beams of different sizes and plotted the results in a double logarithmic diagram of nominal strength versus size. Without attempting a mathematical description, he made the point that this diagram deviates from a straight line of slope -1/2 predicted by LEFM.

An analytical study of size effect due to localization of distributed cracking began in 1976 :331-344; Disc.) (1976;102(EM2). Later, a simple formula of size effect, which describes the size effect for quasi-brittle failures preceded by tests, was derived Bazant (1984) and the crack band model Bazant and Oh (1983) was developed. This model was shown to be in good agreement with the ba-

sic fracture data and size effect data Bazant and Oh (1983), and has been found convenient in programming. However, the crack band model fails to predict crack paths that are not known in advance.

A major advance in concrete fracture was made in 1976 by Hillerborg, Modeer, and Peterson (1976). Inspired by the softening and plastic models of fracture process zone initiated in the works of Barenblatt (1962, 1959) and Dugdale (1960) and developed earlier for materials other than concrete by e.g. Rice (1968); Smith (1974), Hillerborg (1985b,a) improved and adapted the cohesive crack model to concrete. Cohesive crack models were later on coupled to element separation method Ortiz, Leroy, and Needleman (1987); Xu and Needleman (1994) in the context of finite element method. However, the results depend on the mesh unless adaptive remeshing algorithms are used. Meshless methods have been proven a powerful alternative to finite element method. In combination with cohesive crack methods, they give reliably mesh independent results Hao, Liu, Klein, and Rosakis (2004); Li and Simonson (2003); Han and Atluri (2003); Tang, Shen, and Atluri (2003); Liu, Han, Rajendran, and Atluri (2006); Nairn (2003); Guo and Nairn (2004); Maiti and Geubelle (2004); Guz, Menshykov, and Zozulya (2007); Gao, Liu, and Liu (2006); Rabczuk and Areias (2006); Andreaus, Batra, and Porfiri (2005); Le, Mai-Duy, and Tran-Cong (2008); Nishioka (2005); Ma, Lu, and Wang (2006) for complicated problems of concrete fracture.

Meshless methods were pioneered by Atluri and Zhu (1998, 2000); Atluri and Shen (2002), Belytschko, Lu, and Gu (1994b); Belytschko and Tabbara (1996); Belytschko, Krongauz, Organ, Fleming, and Krysl (1996), Liu, Jun,

and Zhang (1995) and other, see e.g. Duarte and Oden (1996); Melenk and Babuska (1996) and were specifically applied to applications involving static and dynamic fracture in continua Hagihara, Tsunori, and Ikeda (2007); Nishioka, Kobayashi, and Fujimoto (2007); Fujimoto and Nishioka (2006); Chandra and Shet (2004); Sladek, Sladek, and Zhang (2007); Rabczuk and Zi (2007); Rabczuk and Belytschko (2005, 2006); Nguyen-Van, N, and Tran-Cong (2008); Chen, Gan, and Chen (2008); Guz, Menshykov, and Zozulya (2007); Krysl and Belytschko (1999); Guo and Nairn (2006); Sladek, Sladek, and Krivacek (2005); Rabczuk and Belytschko (2007); Rabczuk and Eibl (2003); Rabczuk, Belytschko, and Xiao (2004); Maiti and Geubelle (2004); Guz, Menshykov, and Zozulya (2007); Gao, Liu, and Liu (2006); Andreaus, Batra, and Porfiri (2005); Le, Mai-Duy, and Tran-Cong (2008); Ma, Lu, and Wang (2006) and structures Andreaus, Batra, and Porfiri (2005); Rabczuk, Areias, and Belytschko (2007). An excellent book about meshless methods, their applications and abilities is given in Atluri (2002). Meshless methods offer the opportunity to model a discrete crack. Due to the absence of a mesh, the crack can propagate arbitrarily through the discretization. The visibility criterion Belytschko, Lu, and Gu (1994a) and modifications such as the transparency and diffraction method are used to model the kinematics of the crack. One key issue in discrete crack methods is how to track the crack path. This is especially cumbersome for many cracks as they frequently occur in concrete fracture.

Therefore, we employ a discrete crack method that does not need the representation of crack surface. The discrete crack method introduces cohesive crack segment at the nodes. The crack path is represented by a set of cracked nodes. Crack initiation and crack growth can be treated with the same algorithmic procedure. This makes the method especially well suited for studying fracture of concrete. We apply this method to mixed-mode fracture of concrete and show the good agreement between numerical analysis and experimental result.

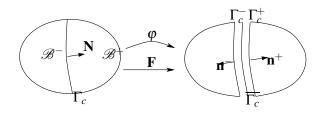The paper is structured as follows: In the next

Figure 1: Kinematics of deformation map

section, we describe the crack model. This includes the derivation of the field equations, the weak form and the discretization. Then, we apply the crack model to concrete fracture, the Nooru-Mohamed (1992) experiment that many concrete researchers used for validation of crack models. At the end, we conclude our paper and give future research directions.

2 Crack Model

2.1 Kinematic Equations

Consider a continuous body $\mathscr{B}$ crossed by a discontinuity Γ_c, figure 1. The deformation φ mapping particles from their original position $\mathbf{X}$ in the reference configuration $\mathscr{B}$ to their current position $\mathbf{x}$ in the deformed configuration $\mathscr{S}$ is introduced on both sides of the discontinuity, $\mathscr{B}^+$ and $\mathscr{B}^-$:

$$\varphi = \begin{cases} \varphi^+ \\ \varphi^- \end{cases} , \quad \mathbf{F} = \begin{cases} \mathbf{F}^+ = \nabla \varphi^+ \; \forall \; \mathbf{X} \in \; \mathscr{B}^+ \\ \mathbf{F}^- = \nabla \varphi^- \; \forall \; \mathbf{X} \in \; \mathscr{B}^- \end{cases}$$

Accordingly, we can introduce independent deformation gradients $\mathbf{F}^+ +$ and $\mathbf{F}^-$ and associated Jacobians $J^+ = det(\mathbf{F}^+)$ and $J^- = det(\mathbf{F}^-)$ on each side of the discontinuity. This parametrization inherently captures jumps $[[\varphi]] = \varphi^+ - \varphi^- \; \forall \; \mathbf{X} \in \Gamma_c$ in the deformation map.

As illustrated in Figure 1, all particles initially located on the unique discontinuity surface Γ_c are mapped onto two surfaces Γ_c^+ and Γ_c^- in the deformed configuration. To uniquely characterize discontinuous failure at finite deformations, the concept of fictitious discontinuity $\overline{\varphi}$ is used. We assume $\overline{\varphi}$ is placed right between the two discontinuity surfaces Γ_c^+ and Γ_c^- in the deformed con-

figuration:

$$\overline{\varphi} = 0.5\left(\varphi^+ + \varphi^-\right),$$
$$\overline{\mathbf{F}} = 0.5\left(\mathbf{F}^+ + \mathbf{F}^-\right) \ \forall \ \mathbf{X} \ \in \ \Gamma_c \tag{1}$$

With these definitions, the normal $\overline{\mathbf{n}} = \overline{J}\overline{\mathbf{F}}^{-t} \cdot \mathbf{N}$ with $\overline{J} = det\overline{\mathbf{F}}$ is obtained by Nanson's formula.

2.2 Equilibrium Equations

The equations of equilibrium is given by

$$div(\mathbf{P}) + \mathbf{b} = \mathbf{0} \ \forall \ \mathbf{X} \ \in \ \mathscr{B}\backslash\Gamma_c \tag{2}$$

where $\mathbf{P}$ and $\mathbf{b}$ is the stress tensor and body force vector, respectively. On the external boundary $\partial\mathscr{B}$ with $\partial\mathscr{B} = \partial\mathscr{B}_u \bigcup \partial\mathscr{B}_t$, $\partial\mathscr{B}_u \bigcup \partial\mathscr{B}_t = \emptyset$ where the subscript u and t denote displacement and traction boundary conditions, the boundary conditions are

$$\varphi \ = \ \tilde{\varphi} \text{ on } \Gamma_u \tag{3}$$
$$\mathbf{P} \cdot \mathbf{N} = \mathbf{T} \ = \ \tilde{\mathbf{T}} \text{ on } \Gamma_t \tag{4}$$

where the tilde denotes superimposed values. On the crack boundary Γ_c, the following equilibrium conditions hold

$$\mathbf{P}^+ \cdot \mathbf{N} = \mathbf{P}^- \cdot \mathbf{N} = \tilde{\mathbf{T}} \ \forall \ \mathbf{X} \ \in \ \Gamma_c \tag{5}$$

2.3 Constitutive Equations

In the bulk, we assume a compressible elastic constitutive behavior of Neo-Hooke type:

$$\sigma = J^{-1}\left(\lambda \ lnJ \ \mathbf{I} - \mu \ \mathbf{I} + \mu \ \mathbf{F} \cdot \mathbf{F}^t\right) \ \forall \ \mathbf{X} \ \in \ \mathscr{B}\backslash\Gamma_c \tag{6}$$

with Lame constants λ and μ and $\mathbf{P} = J\sigma \cdot \mathbf{F}^{-t}$ that relates the Piola stress tensor $\mathbf{P}$ to the Cauchy stress tensor σ.

After cracking, we apply the cohesive crack concept in order to take into account the energy dissipation during crack opening/sliding. The cohesive tractions $\overline{\mathbf{t}}$ in the current configuration can be related to the cohesive tractions $\overline{\mathbf{T}}$ on the undeformed domain through Nanson's formula in terms of area elements da and dA. We assume a

decoupling of the normal and tangential constitutive behavior and use the following cohesive law:

$$\overline{\mathbf{t}} = f_n \exp\left(\frac{-f_n}{G_f}[[\varphi]] \cdot \overline{\mathbf{n}}\right)\overline{\mathbf{n}}$$
$$+ G\left(\mathbf{I} - \overline{\mathbf{n}} \otimes \overline{\mathbf{n}}\right) \cdot [[\varphi]]$$
$$\overline{\mathbf{T}} = \frac{da}{dA}\overline{\mathbf{t}} \ \forall \ \mathbf{X} \ \in \ \Gamma_c \tag{7}$$

In the normal direction, f_n and G_f denote the tensile strength and the fracture energy, respectively. In the tangential direction, G denotes the shear stiffness.

2.4 Weak Form

The weak form can be derived from the strong form by making use of the method of weighted residuals. The weak form is given by: Find $\varphi \in \mathscr{U} \ \forall \delta\varphi \in \mathscr{U}_0$ such that

$$\int_{\mathscr{B}\backslash\Gamma_c} \delta\mathbf{F} : \mathbf{P} \, d\Omega = \int_{\partial\mathscr{B}_t} \delta\varphi \cdot \tilde{\mathbf{T}} \, d\Gamma - \int_{\Gamma_c} [[\varphi]] \cdot \overline{\mathbf{T}} \, d\Gamma \tag{8}$$

with the approximation spaces

$$\mathscr{U} = \left\{\varphi | \varphi \in \mathscr{H}^1, \varphi = \tilde{\varphi} \text{ on } \partial\mathscr{B}_u, \right.$$
$$\left. \varphi \text{ discontinuous on } \Gamma_c\right\} \tag{9}$$
$$\mathscr{U}_0 = \left\{\delta\varphi | \delta\varphi \in \mathscr{H}^1, \delta\varphi = 0 \text{ on } \partial\mathscr{B}_u, \right.$$
$$\left. \delta\varphi \text{ discontinuous on } \Gamma_c\right\} \tag{10}$$

2.5 Discretization

Our formulation is based on the element-free Galerkin method Belytschko, Lu, and Gu (1994b); Rabczuk and Belytschko (2004). For the meshless approximation, it is convenient to decompose the displacement field into continuous parts and discontinuous parts:

$$\varphi = \underbrace{\sum_{J \in \mathscr{W}} N_J(\mathbf{X})\varphi_J}_{\text{continuous}} + \underbrace{\sum_{J \in \mathscr{W}_c} \tilde{N}_J(\mathbf{X})\tilde{\varphi}_J}_{\text{discontinuous}} \tag{11}$$

where $N(\mathbf{X})$ denote the shape functions, $\tilde{N}(\mathbf{X}) = N(\mathbf{X})\Psi(\mathbf{X})$ with enrichment function Ψ, $\mathscr{W}$ are the set of all nodes in the discretization and $\mathscr{W}_c$

are the set of nodes influenced by the crack, i.e. the set of nodes containing the cohesive crack segments. Additional degrees of freedom $\tilde{\varphi}_J$ are introduce to describe the kinematics of the crack. The enrichment function Ψ is chosen such that the shape function $\tilde{N}$ is discontinuous:

$$\Psi(\mathbf{X}) = \begin{cases} 1 \ \forall \ \mathbf{X} \ \in \ \mathcal{B}^+ \\ -1 \ \forall \ \mathbf{X} \ \in \ \mathcal{B}^- \end{cases} \tag{12}$$

Hence, the displacement jump $[[\varphi]]$ depends only on the discontinuous displacement field and is given by

$$[[\varphi]] = 2 \sum_{J \in \mathcal{W}_c} N(\mathbf{X})\tilde{\varphi}_J \tag{13}$$

Note that only nodes that contain cohesive segments are enriched. The cohesive segments pass through the entire domain of influence of the meshless shape function. Hence, no representation of the crack surface is needed that makes the method convenient for many cracks.

The test functions have the same structure:

$$\delta \varphi = \sum_{J \in \mathcal{W}} N_J(\mathbf{X})\delta \varphi_J + \sum_{J \in \mathcal{W}_c} \tilde{N}_J(\mathbf{X})\delta \tilde{\varphi}_J \tag{14}$$

The weak form can now be cast into the following discrete residual statement:

$$\mathbf{R}_J = \mathbf{R}_J^{int} - \mathbf{R}_J^{ext} + \mathbf{R}_J^{coh} = \mathbf{0} \tag{15}$$

with

$$\mathbf{R}_J^{int} = \int_{\mathcal{B} \backslash \Gamma_c} \nabla N_J(\mathbf{X}) \cdot \mathbf{P} \, d\Omega \tag{16}$$

$$\mathbf{R}_J^{ext} = \int_{\mathcal{B} \backslash \Gamma_c} N_J(\mathbf{X})\mathbf{b} \, d\Omega + \int_{\partial \mathcal{B}_t} N_J(\mathbf{X})\tilde{\mathbf{T}} \, d\Gamma \tag{17}$$

$$\mathbf{R}_J^{coh} = \int_{\Gamma_c} N_J(\mathbf{X})\overline{\mathbf{T}} \, d\Gamma \tag{18}$$

By using an incremental iterative Newton-Raphson scheme to solve the non-linear set of equations, Equation (15), we arrive at the following linearized system of equations

$$\mathbf{R}_J^{k+1} = \mathbf{R}_J^k + d\mathbf{R}_J = \mathbf{0} \tag{19}$$

with

$$d\mathbf{R}_J = \sum_{I \in \mathcal{B}} \mathbf{K}_{JI} \, d\varphi_I \tag{20}$$

and the incremental stiffness matrix

$$\mathbf{K}_{JI} = \frac{\partial \mathbf{R}_J}{\partial \varphi_I} = \mathbf{K}_{JI}^{int} - \mathbf{K}_{JI}^{ext} + \mathbf{K}_{JI}^{coh} \tag{21}$$

with

$$\mathbf{K}_{JI}^{int} = \int_{\mathcal{W} \backslash \Gamma_c} \mathbf{B}_J^T \mathbf{C} \mathbf{B}_I \, d\Omega + \int_{\mathcal{W} \backslash \Gamma_c} \mathbf{B}_J^T \cdot \mathbf{P} \cdot \mathbf{B}_I \mathbf{I} \, d\Omega \tag{22}$$

$$\mathbf{K}_{JI}^{ext} = \mathbf{0} \tag{23}$$

$$\mathbf{K}_{JI}^{coh} = \int_{\Gamma_c} N_I(\mathbf{X})\mathbf{T}_\tau N_I(\mathbf{X}) \, d\Gamma$$
$$+ \int_{\Gamma_c} N_I(\mathbf{X})\mathbf{T}_n \cdot \mathbf{G} \cdot \nabla N_I(\mathbf{X}) \, d\Gamma$$
$$+ \int_{\Gamma_c} N_I(\mathbf{X})\overline{\mathbf{T}} \otimes (\mathbf{A} \cdot \mathbf{B}) \, d\Gamma \tag{24}$$

where $\mathbf{B}$ is the matrix that contain the derivatives of the shape functions N and $\tilde{N}$, $\mathbf{C}$ is the tangent stiffness matrix, $\mathbf{K}_{JI}^{ext}$ vanishes since $\mathbf{R}_J^{ext}$ does not depend on φ and the cohesive tangent operators are given by

$$\mathbf{T}_\tau =$$
$$\frac{\partial \overline{\mathbf{t}}}{\partial [[\varphi_n]]} \cdot (\overline{\mathbf{n}} \otimes \overline{\mathbf{n}}) + \frac{\partial \overline{\mathbf{t}}}{\partial [[\varphi_\tau]]} \cdot (\mathbf{I} - \overline{\mathbf{n}} \otimes \overline{\mathbf{n}}) \tag{25}$$

$$\mathbf{T}_n =$$
$$\left(\frac{\partial \overline{\mathbf{t}}}{\partial [[\varphi_n]]} - \frac{\partial \overline{\mathbf{t}}}{\partial [[\varphi_\tau]]} \right) \cdot (\mathbf{n} \otimes [[\varphi]] + [[[\varphi]] \cdot \mathbf{n}] \mathbf{I}) \tag{26}$$

with

$$\frac{\partial \overline{\mathbf{t}}}{\partial [[\varphi_n]]} = \frac{-f_n^2}{G_f} exp \left(\frac{f_n}{G_f} [[\varphi_n]] \cdot \mathbf{n} \right) \mathbf{n} \otimes \mathbf{n} \tag{27}$$

$$\frac{\partial \overline{\mathbf{t}}}{\partial [[\varphi_\tau]]} = d\mathbf{I} \tag{28}$$

and with the second order tensor

$$\mathbf{A} = (\mathbf{I} - \mathbf{n} \otimes \mathbf{n}) \cdot \mathbf{F}^{-t}$$

and fourth order tensor

$$\mathbf{G} = -\mathbf{n} \cdot \left(\mathbf{I} \otimes \overline{\mathbf{F}}^{-t} \right) + \overline{\mathbf{n}} \otimes \overline{\mathbf{n}} \otimes \overline{\mathbf{n}} \cdot \overline{\mathbf{F}}^{-t} \tag{29}$$

For more details on the cohesive law, the reader is referred to Larsson and Fagerstrom (2005).

2.6   Crack criterion

The classical Rankine criterion is used to initiate and propagate crack. Due to the simplicity of our method, crack initiation does not need to be distinguished from crack propagation. To avoid spurious crack path oscillations, a non-local averaging is applied and the maximum principal tensile stress is computed for the averaged stress tensor $\tilde{\sigma}$ rather than the local stress tensor. The averaged stress tensor is computed by

$$\tilde{\sigma} = \frac{\sum\limits_{J \in \mathscr{B}} w_J(\mathbf{X}) \sigma_J}{\sum\limits_{J \in \mathscr{B}} w_J(\mathbf{X})}$$

with weighting function $w_J(\mathbf{X})$. As weighting function, we used the normalized quartic B-spline that is also used within the element-free Galerkin method. The averaged stress tensor is computed in the vicinity of all crack segments.
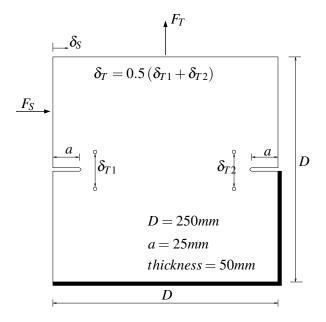
3   Nooru-Mohamed test

Figure 2: Nooru-Mohamed test: experimental setup

Figure 2 depicts the setup of the mixed-mode fracture test of Nooru-Mohamed (1992). A double-notched prism (200 mm × 200 mm × 50 mm)

with two 25 mm deep notches, was loaded simultaneously in tension (T) and shear (S). Various proportional and non-proportional loading paths were followed, with both displacement and load controls. Here we consider loading paths 4 and 6, which are frequently used as benchmarks to check the ability of constitutive models to simulate complex crack paths. Path 4 is non-proportional. The shear force, F_S, is first increased up to a certain value while tensile force F_T is kept zero. Afterwards, the shear force is kept constant while a tensile force is applied under displacement control until the specimen fails completely. In Nooru-Mohamed's experiments, the shear force was kept constant at 5 kN $\approx F_{S,max}/6$ (path-4a), 10 kN $\approx F_{S,max}/3$ (path-4b) and $F_{S,max} = 27.38$ kN (path-4c), where $F_{S,max}$ is the maximum shear force that the specimen could sustain in absence of the tensile force. Paths 6 is, by contrast, proportional, with the ratio of tensile displacement δ_T to shear displacement δ_S being constant. Nooru-Mohamed's tests featured three different values of this ratio: $\delta_T/\delta_S = 1$, $\delta_T/\delta_S = 2$, and $\delta_T/\delta_S = 3$, labeled as path 6a, 6b and 6c, respectively.

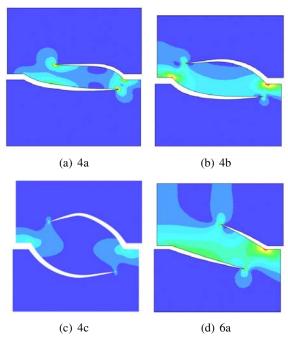| (a) 4a | (b) 4b |
| (c) 4c | (d) 6a |

Figure 3: von Mises stress at the deformed specimen at failure of the Nooru-Mohamed test for different load paths

The material parameters for this problem are Young's modulus E=36.0GPa, Poisson's ratio v=0.22, tensile strength f_n=2.2MPa and fracture energy G_f=100.0N/m. Figure 3 shows the crack path for different loading paths, see above. They agree well with the results reported in Nooru-Mohamed (1992). The associated load-displacement curves are shown in figures 4-7 and match the experiment well. Loading paths 4a and 4b predicts the maximum tensile force reduction due to the presence of the shear force of around 11% and 27% that agrees with the experimental observations of 12% and 29.5%. For loading path 6c, the tensile load carrying capacity is completely lost and the tensile force becomes negative due to the concrete dilatancy. The influence of the mesh refinement for problem 4b is shown in figure 5 for three different meshes: coarse, fine and very fine that correspond to 450 nodes, 1900 nodes and 7600 nodes, respectively. We used unstructured node distributions. The distances between the nodes are approximately the same. The influence of mesh refinement for the other problems is very similar. Concluding, we can say that our method is able to predict the different crack paths and load-displacement behavior very accurately.
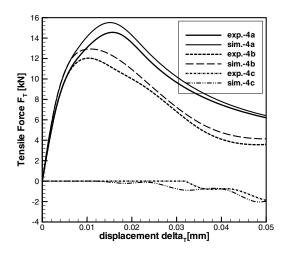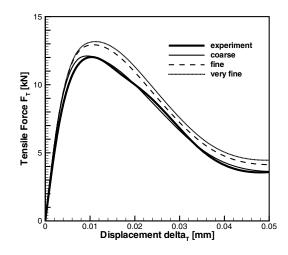

Figure 5: Mesh refinement study for specimen 4b

Figure 6: Tensile Force-displacment curve of the Nooru-Mohamed test for different load paths: 6a, 6b, 6c
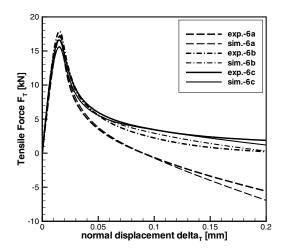

Figure 4: Tensile Force-displacment curve of the Nooru-Mohamed test for different load paths: 4a, 4b, 4c

4   Conclusions

We presented crack growth simulation in concrete structure by simplified meshless discrete crack method. The crack is modeled by set of crack segment. The advantage of modeling the crack as set of disconnected segments is its robustness,
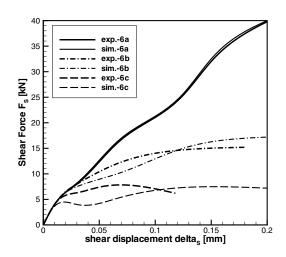
Figure 7: Shear Force-displacment curve of the Nooru-Mohamed test for different load paths: 6a, 6b, 6c

simple implementation and ability to handle many cracks. The latter point is important for cracking in concrete and reinforced concrete.

We studied the Nooru-Mohamed (1992) experiment with complicated crack paths and mixed-mode failure. The results obtained with the method are promising and in close agreement to the experimental data and other more complicated methods proposed in the literature Zi, Rabczuk, and Wall (2007); Patzak and Jirasek (2004). The next step is to study real-world concrete and also reinforced-concrete structures of larger dimensions that failure mechanism is governed by many cracks.

References

Andreaus, U.; Batra, B.; Porfiri, M. (2005): Vibrations of cracked euler-bernoulli beams using meshless local petrov-galerkin (mlpg) method. *CMES-Computer Modeling in Engineering & Sciences*, vol. 9, pp. 111–131.

Atluri, S. (2002): *The Meshless Local Petrov-Galerkin (MLPG) Method*. Tech Science Press.

Atluri, S.; Shen, S. (2002): The meshless local Petrov-Galerkin method: a simple and less-costly alternative to the finite element and boundary element methods. *Computations and Modelling in Engineering and Sciences*, vol. 3, pp. 11–51.

Atluri, S.; Zhu, T. (1998): A new meshless local Petrov-Galerkin (MLPG) approach in computational mechanics. *Computational Mechanics*, vol. 22, pp. 117–127.

Atluri, S.; Zhu, T. (2000): The meshless local Petrov-Galerkin (MLPG) approach for solving problems in elasto-statics. *Computational Mechanics*, vol. 25, pp. 169–179.

Barenblatt, G. (1959): The formation of equilibrium cracks during brittle fracture. general ideas and hypothesis, axially symmetric cracks. *Pritl Mat Mekh*, vol. 23, pp. 434–444.

Barenblatt, G. (1962): The mathematical theory of equilibrium of cracks in brittle fracture. *Advances in Applied Fracture*, vol. 7, pp. 55–129.

Bazant, Z. (1976;102(EM2):331-344; Disc.): Instabilitiy, ductility, and size effect in strain-softening concrete. *J Engng Mech Div, Am Soc Civil Engrs*, vol. 103:, pp. 357–358.

Bazant, Z. (1984): Size effect in blunt fracture: concrete, rock, metal. *J Engng Mech, ASCE*, vol. 110, pp. 518–535.

Bazant, Z.; Oh, B. (1983): Crack band theory for fracture in concrete. *Materials and Structures*, vol. 16, pp. 155–177.

Belytschko, T.; Krongauz, Y.; Organ, D.; Fleming, M.; Krysl, P. (1996): Meshless methods: An overview and recent developments. *Computer Methods in Applied Mechanics and Engineering*, vol. 139, pp. 3–47.

Belytschko, T.; Lu, Y.; Gu, L. (1994): Crack propagation by element-free galkerin methods. *Engineering Fracture Mechanics*, vol. 51, pp. 295–315.

Belytschko, T.; Lu, Y.; Gu, L. (1994): Element-free galerkin methods. *International Journal for*

Numerical Methods in Engineering, vol. 37, pp. 229–256.

Belytschko, T.; Tabbara, M. (1996): Dynamic fracture using element-free galerkin methods. *International Journal for Numerical Methods in Engineering*, vol. 39, no. 6, pp. 923–938.

Chandra, N.; Shet, C. (2004): A micromechanistic perspective of cohesive zone approach in modeling fracture. *CMES-Computer Modeling in Engineering & Sciences*, vol. 5, no. 1, pp. 21–33.

Chen, Z.; Gan, Y.; Chen, J. (2008): A coupled thermo-mechanical model for simulating the material failure evolution due to localized heating. *CMES-Computer Modeling in Engineering & Sciences*, vol. 26, no. 2, pp. 123–137.

Duarte, C.; Oden, J. (1996): An h-p adaptive method using clouds. *Computer Methods in Applied Mechanics and Engineering*, vol. 139, pp. 237–262.

Dugdale, D. (1960): Yielding of steel sheets containing slits. *J Mech Phys Solids*, vol. 8, pp. 100–108.

Fujimoto, T.; Nishioka, T. (2006): Numerical simulation of dynamic elasto visco-plastic fracture using moving finite element method. *CMES-Computer Modeling in Engineering & Sciences*, vol. 11, no. 2, pp. 91–101.

Gao, L.; Liu, K.; Liu, Y. (2006): Applications of mlpg method in dynamic fracture problems. *CMES-Computer Modeling in Engineering & Sciences*, vol. 12, no. 3, pp. 181–195.

Guo, Y.; Nairn, J. (2004): Calculation of j-integral and stress intensity factors using the material point method. *CMES-Computer Modeling in Engineering & Sciences*, vol. 6, no. 3, pp. 295–308.

Guo, Y.; Nairn, J. (2006): Three-dimensional dynamic fracture analysis using the material point method. *CMES-Computer Modeling in Engineering & Sciences*, vol. 16, no. 3, pp. 141–155.

Guz, A.; Menshykov, O.; Zozulya, V. (2007): Contact problem for the flat elliptical crack under normally incident shear wave. *CMES-Computer Modeling in Engineering & Sciences*, vol. 17, no. 3, pp. 205–214.

Hagihara, S.; Tsunori, M.; Ikeda, T. (2007): Application of meshfree method to elastic-plastic fracture mechanics parameter analysis. *CMES-Computer Modeling in Engineering & Sciences*, vol. 17, no. 2, pp. 63–72.

Han, Z.; Atluri, S. (2003): Truly meshless local petrov-galerkin (mlpg) solutions of traction and displacement bies. *Computations and Modelling in Engineering and Sciences*, vol. 4, pp. 665–678.

Hao, s.; Liu, W.; Klein, P.; Rosakis, A. (2004): Modeling and simulation of intersonic crack growth. *International Journal of Solids and Structures*, vol. 41, no. 7, pp. 1773–1799.

Hillerborg, A. (1985): Results of three comparative test series for determining the fracture energy of concrete. *Mater Struct*, vol. 18, pp. 107.

Hillerborg, A. (1985): The theoretical basis of method to determine the fracture energy of concrete. *Mater Struct*, vol. 18, pp. 291–296.

Hillerborg, A.; Modeer, M.; Peterson, P. E. (1976): Analysis of crack formation and crack growth in concrete by means of fracture mechanics and finite elements. *Cement and Concrete Research*, vol. 6, pp. 773–782.

Kaplan, M. (1961): Crack propagation and the fracture concrete. *ACI J*, vol. 58, no. 11.

Kesler, C.; Naus, D.; Lott, J. (1972): Fracture mechanics-its applicability to concrete. *In: Proceedings of the International Conference on the Mechanical Behavior of Materials, Vol. IV, Kyoto, 1971*, vol. The Society of Materials Science, pp. 113–124.

Krysl, P.; Belytschko, T. (1999): The EFGM for dynamic propagation of arbitrary three-dimensional cracks. *International Journal for Numerical Methods in Engineering*, vol. 44, no. 6, pp. 767–800.

Larsson, R.; Fagerstrom, M. (2005): A framework for fracture modelling based on the material forces concept with xfem kinematics. *International Journal for Numerical Methods in Engineering*, vol. 62, pp. 1763–1788.

Le, P.; Mai-Duy, N.; Tran-Cong, T. (2008): A meshless modeling of dynamic strain localization in quasi-brittle materials using radial basis function networks. *CMES-Computer Modeling in Engineering & Sciences*, vol. 25, no. 1, pp. 43–67.

Li, S.; Simonson, B. C. (2003): Meshfree simulation of ductile crack propagation. *International Journal of Computational Methods in Engineering Science and Mechanics*, vol. 6, pp. 1–19.

Liu, H.; Han, Z.; Rajendran, A.; Atluri, S. (2006): Computational modeling of impact response with the rg damage model and the meshless local petrov-galerkin (mlpg) approaches. *Computers Materials and Continua*, vol. 4, pp. 43–53.

Liu, W.; Jun, S.; Zhang, Y. (1995): Reproducing kernel particle methods. *International Journal for Numerical Methods in Engineering*, vol. 20, pp. 1081–1106.

Ma, J.; Lu, H.; Wang, B. (2006): Multiscale simulation using generalized interpolation material point (gimp) method and molecular dynamics (md). *CMES-Computer Modeling in Engineering & Sciences*, vol. 14, no. 2, pp. 101–117.

Maiti, S.; Geubelle, P. (2004): Mesoscale modeling of dynamic fracture of ceramic materials. *CMES-Computer Modeling in Engineering & Sciences*, vol. 5, no. 2, pp. 91–101.

Melenk, J. M.; Babuska, I. (1996): The partition of unity finite element method: basic theory and applications. *Computer Methods in Applied Mechanics and Engineering*, vol. 139, pp. 289–314.

Nairn, J. (2003): Material point method calculations with explicit cracks. *CMES-Computer Modeling in Engineering & Sciences*, vol. 4, no. 6, pp. 649–663.

Nguyen-Van, H.; N, N. M.-D.; Tran-Cong, T. (2008): A smoothed four-node piezoelectric element for analysis of two-dimensional smart structures. *CMES-Computer Modeling in Engineering & Sciences*, vol. 23, no. 3, pp. 209–222.

Nishioka, T. (2005): Recent advances in numerical simulation technologies for various dynamic fracture phenomena. *CMES-Computer Modeling in Engineering & Sciences*, vol. 10, no. 3, pp. 209–215.

Nishioka, T.; Kobayashi, Y.; Fujimoto, T. (2007): The moving finite element method based on delaunay automatic triangulation for fracture path prediction simulations in nonlinear elastic-plastic materials. *CMES-Computer Modeling in Engineering & Sciences*, vol. 17, no. 3, pp. 231–238.

Nooru-Mohamed, M. (1992): *Mixed-mode fracture of concrete: an experimental approach.* PhD thesis, Delft University of Technology, PhD-thesis, 1992.

Ortiz, M.; Leroy, Y.; Needleman, A. (1987): Finite element method for localized failure analysis. *Computer Methods in Applied Mechanics and Engineering*, vol. 61, pp. 189–213.

Patzak, B.; Jirasek, M. (2004): Adaptive resolution of localized damage in quasi-brittle materials. *Journal of Engineering Mechanics ASCE*, vol. 130, pp. 720–732.

Rabczuk, T.; Areias, P. (2006): A meshfree thin shell for arbitrary evolving cracks based on an extrinsic basis. *CMES-Computer Modeling in Engineering & Sciences*, vol. 16, no. 2, pp. 115–130.

Rabczuk, T.; Areias, P.; Belytschko, T. (2007): A meshfree thin shell method for non-linear dynamic fracture. *International Journal for Numerical Methods in Engineering*, vol. 72, no. 5, pp. 524–548.

Rabczuk, T.; Belytschko, T. (2004): Cracking particles: A simplified meshfree method for arbitrary evolving cracks. *International Journal for*

Numerical Methods in Engineering, vol. 61, no. 13, pp. 2316–2343.

Rabczuk, T.; Belytschko, T. (2005): Adaptivity for structured meshfree particle methods in 2d and 3d. *International Journal for Numerical Methods in Engineering*, vol. 63, no. 11, pp. 1559–1582.

Rabczuk, T.; Belytschko, T. (2006): Application of particle methods to static fracture of reinforced concrete structures. *International Journal of Fracture*, vol. 137, no. 19-49, pp. 1559–1582.

Rabczuk, T.; Belytschko, T. (2007): A three-dimensional large deformation meshfree method for arbitrary evolving cracks. *Computer Methods in Applied Mechanics and Engineering*, vol. 196, no. 29-30, pp. 2777–2799.

Rabczuk, T.; Belytschko, T.; Xiao, S. (2004): Stable particle methods based on lagrangian kernels. *Computer Methods in Applied Mechanics and Engineering*, vol. 193, pp. 1035–1063.

Rabczuk, T.; Eibl, J. (2003): Simulation of high velocity concrete fragmentation using sph/mlsph. *International Journal for Numerical Methods in Engineering*, vol. 56, pp. 1421–1444.

Rabczuk, T.; Zi, G. (2007): A meshfree method based on the local partition of unity for cohesive cracks. *Computational Mechanics*, vol. 39, no. 6, pp. 743–760.

Rice, J. (1968): Mathematical analysis in the mechanics of fracture. *In: Liebowitz H, editor. Fracture-and advance treatise, Vol.2, New York, Academic Press.*, pp. 191–308.

Sladek, J.; Sladek, V.; Krivacek, J. (2005): Meshless local petrov-galerkin method for stress and crack analysis in 3-d axisymmetric fgm bodies. *CMES-Computer Modeling in Engineering & Sciences*, vol. 8, no. 3, pp. 259–270.

Sladek, J.; Sladek, V.; Zhang, C. (2007): Fracture analyses in continuously nonhomogeneous piezoelectric solids by the mlpg. *CMES-Computer Modeling in Engineering & Sciences*, vol. 19, no. 3, pp. 247–262.

Smith, E. (1974): The structure in the vicinity of a crack tip: a general theory based on the cohesive crack model. *Engineering Fracture Mechanics*, vol. 6, pp. 213–222.

Tang, Z.; Shen, S.; Atluri, N. (2003): Analysis of materials with strain-gradient effects: A meshless local petrov-galerkin(mlpg) approach, with nodal displacements only. *Computations and Modelling in Engineering and Sciences*, vol. 4, pp. 177–196.

Walsh, P. (1972): Fracture of plain concrete. *Indian Concrete J*, vol. 46, no. 11.

Walsh, P. (1976): Crack initiation in plain concrete. *Mag Concrete Res*, vol. 28, no. 37-41.

Xu, X.-P.; Needleman, A. (1994): Numerical simulations of fast crack growth in brittle solids. *Journal of the Mechanics and Physics of Solids*, vol. 42, pp. 1397–1434.

Zi, G.; Rabczuk, T.; Wall, W. (2007): Extended meshfree methods without branch enrichment for cohesive cracks. *Computational Mechanics*, vol. 40, pp. 367–382.